



LAWRENCE  
LIVERMORE  
NATIONAL  
LABORATORY

# Application of Ab Initio and CALPHAD Thermodynamics to Mo-Ta-W Alloys

P. E. A. Turchi, V. Drchal, J. Kudrnovsky, C. Colinet, L. Kaufman, Z-K. Liu

November 12, 2004

Physical Review B

## **Disclaimer**

---

This document was prepared as an account of work sponsored by an agency of the United States Government. Neither the United States Government nor the University of California nor any of their employees, makes any warranty, express or implied, or assumes any legal liability or responsibility for the accuracy, completeness, or usefulness of any information, apparatus, product, or process disclosed, or represents that its use would not infringe privately owned rights. Reference herein to any specific commercial product, process, or service by trade name, trademark, manufacturer, or otherwise, does not necessarily constitute or imply its endorsement, recommendation, or favoring by the United States Government or the University of California. The views and opinions of authors expressed herein do not necessarily state or reflect those of the United States Government or the University of California, and shall not be used for advertising or product endorsement purposes.

# **Application of *Ab Initio* and CALPHAD Thermodynamics to Mo-Ta-W Alloys**

P. E. A. Turchi

*Lawrence Livermore National Laboratory, L-353, P.O. Box 808, Livermore, CA 94551, USA*

V. Drchal and J. Kudrnovský

*Institute of Physics, Academy of Sciences of the Czech Republic, Na Slovance 2, CZ-180 40 Praha  
8, Czech Republic*

C. Colinet

*LTPCM-ENSEEG, Domaine Universitaire, BP 75, F-38402 Saint Martin d'Hères, France*

Larry Kaufman

*Dept. of Materials Science and Engineering, MIT, Cambridge, MA 02139*

Zi-Kui Liu

*Dept. of Materials Science and Engineering, The Pennsylvania State University, University  
Park, PA 16803*

(October 8, 2004)

## **Abstract**

A parameter-free electronic structure approach is applied to the study of stability and chemical order in substitutional bcc-based Mo-Ta, Ta-W and Mo-W alloys. The method is based on a Green function description of the electronic structure of random alloys. Configurational order is treated within

the generalized perturbation method, and temperature effects are accounted for by a generalized mean-field approach. The practical application of this study to phase stability in Mo-Ta-W alloys is tested by converting the *ab initio* output thermodynamics of the three binary subsystems to a format amenable to a CALPHAD treatment. The results of this conversion are then used to predict isothermal sections of the ternary phase diagram of the Mo-Ta-W system that are compared with the results obtained directly from the *ab initio* approach with the cluster variation method. It is concluded that the proposed CALPHAD conversion of the *ab initio* results is a viable scheme to capture the alloy properties predicted from first-principles electronic structure calculations.

61.66.Dk, 64.60.Cn, 71.20.Be, 81.30.Bx

## I. INTRODUCTION

According to the assessed phase diagrams of the Mo-W, Mo-Ta, and Ta-W systems, the pure elements form in the solid phase a continuous series of body centered (bcc or A2, or  $\alpha$ ) solid solutions with each other, with no existence of intermediate phases or superlattices [1]. However indications exist that at least two of these alloys should display chemical order. For Mo-Ta alloys, it has been observed that the evolution of the lattice parameter with alloy composition exhibits a negative departure from Vegard's law [2–4]. Note that the positive departure observed in Ref. [5] has been attributed to the neglect of the measurement of the molybdenum weight loss in the samples. In addition, the relative magnitude of the peak heights as a function of alloy composition measured by X-ray diffraction has been attributed to short-range order (SRO) [3]. This SRO combined with size effect has been associated with the cleavage fracture of Mo-Ta alloys located in the central region of the phase diagram. Finally, the activities of Ta and Mo exhibit large negative deviations from ideality (Raoult's law), and the overall measured thermodynamic properties between 1000 K and 1300 K [5] are compatible with the existence of SRO. These sparse experimental facts have led us to reexamine this alloy system with a first-principles approach to stability and chemical order. Similar experimental findings have been reported in the literature for the Ta-W system [6,7], and a recent first-principles analysis has led to the prediction of two ordered phases, namely B2 around equi-atomic composition and  $D0_3$  around  $TaW_3$  and  $Ta_3W$  [8]. Except for the determination of the solidus-liquidus line, very few results are available about the solid-phase portion of the phase diagram of Mo-W alloys.

Hence in this paper, the study has been extended to Mo-Ta and Mo-W with a similar first-principles approach to examine the ternary Mo-Ta-W alloy. The configurational order has been formulated within the Generalized Perturbation Method (GPM) [9–12]. The electronic properties of the reference medium on which the GPM relies were described in the framework of the self-consistent tight-binding-linear muffin-tin orbital (TB-LMTO) multiple scattering formulation of the Coherent Potential Approximation (CPA) [12,13]. Finally,

temperature effects on local order and stability were accounted for by means of a standard generalized mean-field approach, namely the cluster variation method (CVM) [10,14]. From the first-principles thermodynamic analysis, Mo-Ta alloys should exhibit a definite tendency toward order with a B2 (or  $\alpha'$ ) superstructure of CsCl-type. The theoretical analysis also reveals a low-lying phase diagram that supports the experimental findings discussed above. The critical order (B2)-disorder (A2) line exists below 1772 K with a maximum transition temperature around 47 at.% Ta. Similar findings have been reported in the case of Ta-W alloys with a maximum critical B2-A2 around 57 at.% W and slightly below 1000 K [8]. For all practical purposes, we will neglect in the following the existence of a  $D0_3$  ordered structure that exists below 200 K around  $TaW_3$  and 100K around  $Ta_3W$ , since this long-range order (LRO) can never be observed (the energetics associated with the SRO of  $D0_3$ -type is quite negligible at temperatures where this alloy can find applications). Finally, our results show that the Mo-W alloy system should exhibit a negligible heat of formation and almost no SRO as would be expected for an ideal solid solution.

Before analyzing the data for the ternary Mo-Ta-W alloy (for which no data, assessed or measured, are available) the results from *ab initio* calculations indicate that two of the binary subsystems, Mo-Ta and Ta-W, exhibit a tendency towards order with a broad range of stability of the B2 ordered phase below 1770 K and 1000 K, respectively, whereas Mo-W behaves like an ideal solid solution. Prior to the investigation of the phase diagram of the ternary alloy, the predicted output thermodynamic information deduced from *ab initio* calculations for Mo-Ta and Ta-W will be converted in a Redlich-Kister/Bragg-Williams format [15,16] to express the Gibbs energy of each binary alloy in a form amenable to a so-called CALPHAD (CALculation of PHase Diagrams) thermodynamic treatment [17–19]. This conversion will then allow us to explore the impact of the predicted chemical order in the binaries on ternary-phase equilibrium, and to predict isothermal sections of the ternary phase diagram of Mo-Ta-W. The phase diagram results compare advantageously to those obtained from a CVM treatment directly applied to the ternary system with input energetics from the *ab initio* calculations. It is worth noting that since all three pure metals and their

binary combinations are stable in the bcc structure, the questions that may arise about lattice stability [18–20] between the results of the *ab initio* approach and CALPHAD do not apply here.

The paper is organized as follows. In section II, we discuss the electronic structure and equilibrium properties of Mo-Ta, Mo-W, and Ta-W alloys based on a first-principles TB-LMTO-CPA description of the electronic structure of disordered alloys. In section III we present the results of the ground-state analysis of the Ising Hamiltonian based on a treatment of ordering within the GPM. In section IV the influence of temperature on stability and local order is studied with a standard generalized mean-field approach and the predicted coherent phase diagrams are presented. Then in section V, we show how the thermodynamic information obtained from *ab initio* can be used to cast the Gibbs energy for each phase of the three binaries in a CALPHAD format to give properties that favorably compared with those directly derived from *ab initio*. In section VI, the CALPHAD approach is used to describe the thermodynamics of the ternary Mo-Ta-W alloys, and the results on some isothermal sections of the ternary phase diagram are discussed with and without direct input from *ab initio* calculations for comparison sake. The CALPHAD ternary phase diagram of Mo-Ta-W is compared with the one obtained from the direct application of the CVM to the ternary system with the input energetics from the binary subsystems obtained from *ab initio*. Finally, in section VII, conclusions are drawn on the validity and potential applications of this procedure.

## II. ELECTRONIC STRUCTURE AND EQUILIBRIUM PROPERTIES

In a previous study we reported the electronic structure properties of Ta-W based on a proper treatment of the disordered alloys [8]. Since the single-site CPA, expressed with the Green’s function formalism and implemented within the TB-LMTO-CPA [12], provides an appropriate basis, the same methodology has been applied to the other binaries Mo-Ta and Mo-W for completeness. The electronic structure calculations were carried out on the

basis of the charge self-consistent fully relativistic version of the TB-LMTO-CPA method within the atomic sphere approximation (ASA) and the local density approximation (LDA) of density functional theory. The LDA calculations were based on the exchange-correlation energy of Ceperley and Alder [21] as parameterized by Perdew and Zunger [22]. To eliminate the charge transfer effects, at each lattice parameter and alloy composition, the atomic sphere radii of the two species were adjusted in such a way that atoms were charge neutral while preserving the total volume of the alloy. In our calculations we used 168  $\mathbf{k}$ -points in the irreducible wedge of the Brillouin zone to perform the integrations that are necessary during the self-consistent calculations, and 2320  $\mathbf{k}$ -points in the full Brillouin zone for the calculation of the effective cluster interactions within the GPM. We use 12 energy points on a semi-circle in the upper half-plane of complex energy to perform the energy integration using Gauss' method. The densities of states (DOS) were evaluated on a line 0.005 Ry above the real axis (with an energy step of about 5 mRy) and then deconvoluted on the real axis. The CPA equations were solved iteratively using the method described in Ref. [12].

In Fig. 1 we display the DOS of the alloy species and of the chemically random alloys at equi-atomic composition. Although the DOS of the three transition metals are similar, note that, at the Fermi energy, the DOS of Ta is located in a region of high density, whereas those of Mo and W are in the pseudo-gap region. This simply reflects the variation of the number of valence electrons  $N_v$  from 4 for Ta to 5 for Mo and W. The minor differences in the DOS of Mo and W can be solely attributed to the difference in electronic properties between the 4d and 5d series, and mostly to relativistic effects. The overall shape of the DOS is preserved in the alloy cases. However, the DOS of the two equi-atomic alloys TaMo and TaW display a stronger effect due chemical disorder since the difference in the numbers of valence electrons  $\Delta N_v$  is equal to unity, as opposed to 0 in the MoW case. At this composition, the Fermi energy of TaMo and TaW correspond to  $N_v = 4.5$  whereas the one of MoW is kept fixed at  $N_v = 5$  pretty much at the same location in the pseudo-gap as in the case of the pure metals Mo and W. Since disorder is minimal for these alloys, the deep minimum observed in the DOS still corresponds to a clear separation between bonding



and anti-bonding states in the alloy band structure, and the overall DOS remain practically unchanged with alloy composition. Thus the variation of the electronic structure properties with alloy composition is almost entirely reflected in the variation of  $N_v$ , and therefore in the location of the Fermi energy as would be the case for an alloy treated within the virtual crystal approximation.

In Fig. 2, we show the departure from Vegard's law, given by  $\delta a^{\text{eq}} = a_{\text{alloy}}^{\text{eq}} - \sum_i c_i a_i^{\text{eq}}$ , where  $a_i^{\text{eq}}$  is the equilibrium lattice constant of the pure element  $i$ , for the three chemically random alloys at composition  $c_i$  and equilibrium lattice parameter  $a_{\text{alloy}}^{\text{eq}}$ . We also report the curves obtained from the experimentally measured lattice parameter (in Å) versus composition represented by  $a = 3.164 + 0.1054 c_{\text{Ta}} + 0.03226 c_{\text{Ta}}^2$  [6] in the case of Ta-W, and by  $a = 3.146 + 0.1209 c_{\text{Ta}} + 0.03398 c_{\text{Ta}}^2$  in the case of Ta-Mo [2,4]. Note that the equilibrium lattice parameters of Ta, Mo, and W from these calculations are 3.2806, 3.1738, and 3.1808 Å, compared with the experimental values of 3.3009, 3.146, and 3.164 Å, respectively. Although there is about a 1% discrepancy between the theoretical and experimental values of lattice constant, the departure from Vegard's law are well reproduced. The results suggest that alloy formation is favored, at least in the case of Ta-Mo and Ta-W, and should lead to a denser structure than a simple combination of both alloy species would.

Figure 3 displays the variation of the bulk modulus for each of the chemically random alloys with composition. For the pure elements, there is a typical 15% discrepancy between predicted and measured values. One should note that, as observed experimentally, a one-valence electron difference leads to a 50% (35%) increase in the bulk modulus when going from Ta to W (Mo).

For comparison purposes, we report in Table I the equilibrium lattice constant and bulk modulus for the pure species, obtained by two *ab initio* approaches. Method 1 refers to the standard scalar relativistic LMTO-ASA [23] with inclusion of so-called combined corrections that account for overlap of atomic spheres and for higher partial waves inside the atomic spheres, and with exchange and correlation potential proposed by von Barth and Hedin [24]. Method 2 corresponds to the fully relativistic TB-LMTO-ASA-CPA [12], that has been

selected in this work for its applicability to off-stoichiometric alloys (including the pure elements), whereas method 1 is only applicable to stoichiometric alloys (and pure elements) describable by supercells. Note that both methods give values for the lattice constant and the bulk modulus which are within the error expected from any LDA calculation.

Finally in Fig. 4 we show the variation of the formation (or mixing) energy of the chemically random alloy with composition. This energy for an A-B alloy is given by

$$\Delta E_{\text{mix}} = E_{\text{alloy}}^{\text{CPA}} - \sum_i c_i E_i^{\text{eq}} \quad (2.1)$$

where  $E_{\text{alloy}}^{\text{CPA}}$  is the total energy of the alloy described within the CPA at its equilibrium lattice parameter, and  $E_i^{\text{eq}}$  is the total energy of pure species  $i$  at its corresponding equilibrium lattice parameter. This mixing energy is negative in the case of Ta-W and Ta-Mo with a maximum value of  $-12.292$  and  $-17.670$  kJ/mol at a tantalum composition of about 0.375 and 0.433, respectively (To make contact with the CALPHAD results, J/mol is adopted as the units of energy). Note that in the case of Mo-W the maximum mixing energy is -51 J/mol, *i.e.*, zero for all practical purposes. Hence, the energetics favors the formation of the disordered alloy configuration in the whole range of alloy composition for Ta-Mo and Ta-W alloys. On the other hand, Mo-W behaves like an ideal solid solution. Our results confirm a previous conclusion drawn from a semi-empirical tight-binding estimation of the energy of formation of the random Ta-W and Ta-Mo alloys as a function of composition [25]. However in this study, the tight-binding energies are way underestimated, and the general evolution of the formation energy with alloy composition does not reveal any asymmetry as it should since the DOS at the Fermi energy that controls the strength of the bonding in these two alloys varies significantly with composition (*i.e.*, the number of valence electrons). Once again, since Ta-Mo and Ta-W are iso-electronic, the difference in the bond strength can solely be attributed to relativistic effects that impact band hybridization [26]. Note that the tight-binding analysis of the energetics of Mo-W, in full agreement with the present results, suggests a negligible contribution of d-band mixing to the mixing energy since  $\Delta N_v = 0$  [25,27].

### III. GROUND-STATE PROPERTIES

Within the GPM [9–12], the quantum mechanical description of the alloy energetics is mapped onto an Ising model by expressing the formation energy of an alloy  $A_{1-c}B_c$  in a particular configuration  $\mathcal{C}$  as the sum of two terms: a configuration-independent but composition-dependent term,  $\Delta E_{\text{dis}}(c)$ , that is associated with a reference medium, and a configuration-dependent term, the ordering energy  $\Delta E_{\text{ord}}^{\mathcal{C}}(\{p_n\})$ , that can be expanded to lowest order in perturbation in terms of pair interactions that are composition dependent according to

$$\Delta E_{\text{ord}}(\{p_n\}) = \frac{1}{2} \sum_{n,m \neq n} V_{nm} \delta c_n \delta c_m \quad (3.1)$$

where  $\delta c_n$  refers to the fluctuation of composition at site  $n$ ,  $\delta c_n = p_n - c$ , where  $c$  is the concentration in B-species, and  $p_n$  is an occupation number associated with site  $n$ , equal to 1 or 0 depending on whether or not the site is occupied by a B-species. The  $V_{nm}$  corresponds to an effective pair interaction between site  $n$  and  $m$  that is composition dependent and is given by the combination  $V_{nm}^{\text{AA}} + V_{nm}^{\text{BB}} - 2V_{nm}^{\text{AB}}$ . At zero temperature Eq.(3.1) takes the simple form

$$\Delta E_{\text{ord}}(\{q_s\}) \simeq \sum_s q_s V_s \quad (3.2)$$

with  $q_s = \frac{c}{2}(n_s^{\text{BB}} - cn_s)$ , where  $n_s^{\text{BB}}$  and  $n_s$  refer to the number of BB pairs and the total number of pairs per site, respectively, associated with the  $s^{\text{th}}$ -neighbor shell, and  $c$  is the concentration in B species. In this last equation,  $V_s$  represents a  $s^{\text{th}}$ -neighbor effective pair interaction (EPI). Hence, the sign convention that has been adopted is such that when  $V_s > 0$  ( $< 0$ ), AB (AA or BB) pairs associated with a species at the origin and the other in the  $s^{\text{th}}$ -neighbor shell are favored.

As seen from Eq.(3.2), any alloy configuration is specified by a unique set of parameters  $\{q_s\}$  that only depends on site occupancies. For example, at zero temperature and for  $s = 1-5$ , these parameters take the values  $-1, 3/4, 3/2, -3, 1$  for B2 order (of CsCl-type) at

equi-atomic composition and  $-1/4$ ,  $-3/16$ ,  $9/8$ ,  $-3/4$ ,  $-1/4$  for  $D0_3$  order (of  $\text{Fe}_3\text{Al}$ -type) at  $c = 1/4, 3/4$ . For all three alloy systems, the EPIs were computed from the knowledge of the electronic structure of the chemically random state within the CPA that is chosen as the reference medium at each composition and lattice parameter [9–11]. In Fig. 5 the first and second neighbor pair interactions,  $V_1$  and  $V_2$ , are plotted as functions of alloy composition at the equilibrium lattice parameter and Fermi energy of the corresponding chemically random alloy. The more distant EPIs ( $V_s$ ,  $s \geq 3$ ), at least an order of magnitude smaller than the first two EPIs, contribute very little to the ordering energy. Also the variation of lattice parameter (and therefore pressure) has a negligible influence on the magnitude of the EPIs at any alloy composition.

The results of a ground-state analysis of the Ising model applied to the bcc lattice [10,28–31], together with the magnitude and sign of the EPIs displayed in Fig. 5 lead to the prediction of the most probable ground states at zero temperature. In the case of Ta-W alloys, two ground states exist: the  $D0_3$  ordered phase for  $\text{TaW}_3$ , and to a less extent  $\text{Ta}_3\text{W}$ , and the B2 ordered phase for TaW, with the corresponding ordering energies equal to about  $-2.035$ ,  $-1.076$ , and  $-5.340$  kJ/mol, respectively [8]. For Mo-Ta alloys, only a B2 ordered state at equi-atomic composition is found with an ordering energy of about  $-8.446$  kJ/mol. Overall, the ordering tendencies are stronger for the W-rich Ta-W and Mo-rich Ta-Mo alloys, and this trend is consistent with what is expected for transition metal alloys [10,11]. Indeed, the variation of the dominant EPIs with the number of d-electrons displays in general two zeros that are located around 3 and 7 d-electrons, with a positive sign of the EPIs in the central region (that indicates an ordering trend). Although the location of the zeros varies with the scattering properties of the electrons and alloy composition, hetero-atomic pairs are increasingly favored when the number of d-electrons increases from Ta (about 3.3) to Mo or W (about 4.4) in the Ta-Mo or Ta-W case, which is what Fig. 5 shows in a more quantitative way. Since Mo and W are iso-electronic, diagonal disorder effects are negligible and the ordering trend is rather negligible. In the case of Mo-W, with  $V_1 < 0$  and  $V_2 > 0$ , the prediction of a slight tendency towards phase separation confirms the conclusions drawn

from a semi-phenomenological tight-binding approach [25,27].

To confirm the GPM predictions, calculations were performed with method 1, LMTO-ASA, mentioned in section II, and compared with those of method 2, *i.e.*, TB-LMTO-ASA-CPA-GPM, to study the equilibrium properties and the energetics of the ordered B2 phase of  $\text{Ta}_{50}\text{W}_{50}$ . In the case of method 2, the energy of formation of the ordered configuration B2 is given by  $\Delta E_{\text{form}}^{\text{B2}} = \Delta E_{\text{mix}} + \Delta E_{\text{ord}}^{\text{B2}}$ , see Eqs. (2.1) and (3.2). The equilibrium lattice constant of the B2 phase was obtained by minimizing the energy  $\Delta E_{\text{form}}^{\text{B2}}$  with respect to volume since, from the CPA and the GPM calculations, the variation with volume of  $\Delta E_{\text{mix}}$  and of the EPIs that built up the ordering energy  $\Delta E_{\text{ord}}^{\text{B2}}$  are known. The results of both methods, reported in Table I, are consistent in the sense that the formation energy of the ordered B2 phase, of the order of  $-11$  and  $-17$  kJ/mol from methods 1 and 2, is negative, and therefore favors phase formation. The variation in the results, within the error expected from any LDA calculation, reflects the various levels of approximation that characterize each method: form of exchange-correlation potential, and scalar relativistic versus fully relativistic treatment. However, one can note that the departure of the lattice constant from Vegard's law given by both methods is about  $-0.008$  Å, once again consistent with a tendency towards alloy formation and order. These ordering trends confirm previous analysis performed within tight-binding [25] and with full-potential LMTO electronic structure calculations [8] in the case of Ta-W alloys, and with the VASP implementation [32] of pseudo-potential electronic structure method [33] and tight-binding analysis [27,34] in the case of Ta-Mo.

#### IV. STABILITY AT FINITE TEMPERATURE

By making use of the energetics presented in sections II and III the Ising model has been solved with the CVM [10,14]. At each temperature and alloy composition, the configurational part of the free energy has been minimized with a Newton-Raphson technique. For the bcc-based alloys considered here, the irregular tetrahedron made of four first and two second-nearest-neighbor pairs [35] was considered as the maximum cluster that characterizes

the level of approximation of the CVM. This cluster allows a proper statistical treatment with the EPIs  $V_1$  and  $V_2$  included in the pair expansion of the Ising model, an approximation which is justified here since the more distant EPIs have negligible amplitude. The predicted phase diagrams of Ta-Mo and Ta-W are presented in Fig. 6. Considering the high melting point of the alloy species, the B2 ordered phase of Ta-W and Ta-Mo alloys are stable at low temperature, not exceeding 1000 K and 1800 K, respectively. More details about the Ta-W phase diagram can be found in Ref. [8] where the region of stability of the  $D0_3$  ordered structure below room temperature is discussed. The asymmetry of both phase diagrams is a direct consequence of the alloy energetics that exhibits an extremum in the mixing energy, see Fig. 4, and stronger ordering trends, see Fig. 5, for W-rich and Mo-rich Ta-based alloys. In what follows, for all practical purposes, we will ignore the existence of the  $D0_3$  phase in the case of the Ta-W system, and will assume that the Mo-W alloy behaves like an ideal solid solution since its phase diagram in the solid phase displays a miscibility gap well below room temperature. Note also that despite the noticeable difference in the elastic properties of Ta, Mo, and W, the vibrational free energy estimated from a simple Debye theory [36] is more than an order of magnitude smaller than the CVM free energy, and therefore has little effect on the predicted phase diagrams displayed in Fig. 6.

In summary, for both Ta-W and Ta-Mo alloys, the existence of a region of B2 order in the phase diagram is predicted. This finding obviously translates in a negative departure of the species-resolved activities [37] from linearity as a function of alloy composition (Raoult's law), as confirmed experimentally in the case of Ta-W [7,8]. In the present study, the departure from linearity not only indicates a tendency towards formation of the Ta-W and Ta-Mo solid solutions but also chemical short-range order (SRO). Only one x-ray diffraction investigation reports in the case of Ta-Mo the existence of SRO with peak maxima near the (100) and (300) reciprocal lattice positions that are indicative of a B2 signature [3]. Anomalous dispersion X-ray diffuse scattering measurements at a synchrotron source (in the case of Ta-Mo alloys) or neutron diffraction experiments (for Ta-W alloys) are highly desirable, and should reveal unambiguously the nature of the short-range order on samples

well annealed at relatively high temperature to promote the thermally activated ordering process. Meanwhile, experimental evidence for such trends can be challenging since slow kinetics at relatively low temperature can obliterate the observation of long-range order in these refractory alloys. The only positive point to make is that since the B2→A2 transition is second order, one should expect strong diffuse scattering intensities well above the critical order-disorder temperature and away from stoichiometry, as was shown in the case of Ta-W alloys [8]. Finally, note that cleavage behavior is found for Ta-Mo and Ta-W whereas in the case of Mo-W flow behavior [5] is observed. This change in mechanical response is consistent with the difference in the ordering trends that are predicted here.

## V. *AB INITIO* INPUT TO CALPHAD ALLOY THERMODYNAMICS

In this part of the study we are aiming at describing the thermodynamics of the binary systems obtained from *ab initio* calculations with the CALPHAD formalism so that assessment of the stability properties of the ternary alloy can be easily carried out. We will show that by supplementing the thermo-chemical database with information from *ab initio*, CALPHAD-based calculations for higher-order component alloys can lead to useful prediction that can guide experiments. The coupling of phase diagram calculations and thermo-chemistry makes CALPHAD a powerful tool to predict the thermodynamic properties of complex multi-component materials [19,38–40]. For the pure elements, we will consider the formulation suggested by the Scientific Group Thermodata Europe (SGTE) [41] that gives the Gibbs energy  ${}^0G_i^\Phi(T)$  of each element  $i$  in a particular phase  $\Phi$  with reference to the enthalpy  $H_i^{\text{SER}}(298.15\text{K})$  of element  $i$  in a standard element reference state (SER is usually taken as the ground-state structure) at 298.15 K and ambient pressure. These Gibbs energies, expressed as functions of temperature, can be found in Ref. [42]. For a substitutional binary phase (the liquid phase and the bcc-A2 solid solution in the present case), the Gibbs energy is defined as [19,38,40]

$$G^\Phi(\{c_i\}, T) = {}^{\text{ref}} G^\Phi(\{c_i\}, T) + {}^{\text{id}} G^\Phi(\{c_i\}, T) + {}^{\text{xc}} G^\Phi(\{c_i\}, T) \quad (5.1)$$

where  $c_i$  is the molar fraction of species  $i$  in the phase  $\Phi$ . In this equation the first term represents the concentration-weighted average molar Gibbs energies of the pure elements, the second term is the ideal molar Gibbs energy of mixing (*i.e.* the mixing entropy contribution), and the last term is the excess Gibbs energy due to non-ideal contributions given by the Muggianu expression [43]. More explicitly the three terms are given by the following equations

$$\begin{aligned} {}^{\text{ref}}G^{\Phi}(\{c_i\}, T) &= \sum_i c_i {}^0G_i^{\Phi}(T) \\ {}^{\text{id}}G^{\Phi}(\{c_i\}, T) &= RT \sum_i c_i \ln c_i \\ {}^{\text{xs}}G^{\Phi}(\{c_i\}, T) &= \sum_i \sum_{j \neq i} c_i c_j \sum_{p=0, n} {}^pL_{i,j}^{\Phi}(T) (c_i - c_j)^p \end{aligned} \quad (5.2)$$

where  ${}^pL_{i,j}^{\Phi}(T)$  is the  $p$ -th order binary interaction parameter expressed as a polynomial in temperature  $T$  that contributes to the so-called Redlich-Kister expansion [44].

To describe the ordered alloy A-B in the B2 phase we will consider a two-sublattice model [45–47] that leads to the definition of the three terms entering Eq.(5.1) as follows

$$\begin{aligned} {}^{\text{ref}}G^{\Phi}(\{y_i^s\}, T) &= \sum_{i,j} y_i^{\text{I}} y_j^{\text{II}} {}^0G_{i,j}^{\Phi}(T) \\ {}^{\text{id}}G^{\Phi}(\{y_i^s\}, T) &= RT \sum_{s=\text{I,II}} N_s \sum_i y_i^s \ln y_i^s \\ {}^{\text{xs}}G^{\Phi}(\{y_i^s\}, T) &= y_{\text{A}}^{\text{I}} y_{\text{B}}^{\text{I}} \sum_i y_i^{\text{II}} \sum_{p=0, n} {}^pL_{\text{A,B};i}^{\Phi} (y_{\text{A}}^{\text{I}} - y_{\text{B}}^{\text{I}})^p + y_{\text{A}}^{\text{II}} y_{\text{B}}^{\text{II}} \sum_i y_i^{\text{I}} \sum_{p=0, n} {}^pL_{i;\text{A,B}}^{\Phi} (y_{\text{A}}^{\text{II}} - y_{\text{B}}^{\text{II}})^p \end{aligned} \quad (5.3)$$

where

$${}^0G_{i,j}^{\Phi} = N_{\text{I}} {}^0G_i^{\text{SER}} + N_{\text{II}} {}^0G_j^{\text{SER}} + \Delta G_{i,j}^{\Phi} \quad (5.4)$$

and  $y_i^s$  is the fractional site occupation of species  $i$  on sublattice  $s$  given by the ratio  $n_i^s/N_s$ , with  $n_i^s$  and  $N_s$  representing the number of atoms of species  $i$  and the total number of sites on sublattice  $s$ , respectively. In Eq.(5.3)  ${}^pL_{\text{A,B};i}^{\Phi}$  is the  $p$ -th order interaction parameter between species A and B on the first sublattice with species  $i$  on the second sublattice (note that a colon separates species occupying different sublattices whereas a comma separates species that interact on the same sublattice). As usually assumed  ${}^pL_{i,j;k}^{\Phi} = {}^pL_{i,j;k'}$ . In the case of the B2 compound the Gibbs energy is expressed as



$$G^{\text{bcc-B2}}(\{c_i\}, T) = G^{\text{bcc-A2}}(\{c_i\}, T) + \Delta G^{\text{ord}}(T) \quad (5.5)$$

where  $G^{\text{bcc-A2}}(\{c_i\}, T)$  is given by Eqs.(5.1) and (5.2), and the ordering energy,  $\Delta G^{\text{ord}}(T)$ , is written as

$$\Delta G^{\text{ord}}(T) = {}^{\text{xs}} G^{\text{ord}}(\{y_i^s\}, T) - {}^{\text{xs}} G^{\text{ord}}(\{c_i^s\}, T) \quad (5.6)$$

with  ${}^{\text{xs}} G^{\text{ord}}(\{c_i^s\}, T)$  given by Eq.(5.3).

For both Ta-W and Ta-Mo alloys, a one-sublattice model is considered for the liquid phase and the bcc-A2 solid solution whereas a two-sublattice model describes the thermodynamics of the bcc-B2 ordered phase. The Gibbs energies and molar enthalpies of formation of the bcc phases (between 800 and 3000 K for Ta-W, and 1500 and 3000 K for Ta-Mo) as well as the location of the second-order critical line that delineates the region of stability of the B2 phase, as obtained from the CVM minimization with the energetics calculated from *ab initio*, have been considered as input information for the fitting procedure. The procedure itself made use of the PARROT module [48] of the Thermo-Calc application software [49]. Finally to match the energetics between the bcc-A2 solid solution and the liquid phase we assumed that the Redlich-Kister parameters of the two phases were the same except for an extra contribution to  ${}^0 L_{\text{A,B}}^{\text{liq}}$  for the sake of simplicity. Hence, this procedure ensures that the  $T_0$  temperature, that is defined by the equality of the Gibbs energies of the liquid and the bcc-A2 solid solution at equi-atomic composition, is compatible with the experimental and CALPHAD assessed data on the liquidus-solidus lines [1]. The results of the fit are given in the appendix [50], and the output of the procedure just described will be referred to as *ab initio*-CALPHAD in what follows. As illustrated in Fig. 7 for Ta-Mo alloys the molar Gibbs energies and enthalpies of formation (solid lines) obtained from the fitting procedure reproduce very well the CVM results in a broad range of temperatures, and well within the range of accuracy accepted in a CALPHAD assessment of experimental data. To compensate for the simple Bragg-Williams approximation the temperature dependence of the Redlich-Kister (or interaction) parameters gives ample flexibility to reproduce low- and high-temperature results at the same time. The fact that SRO is not well accounted for is

most seen in Fig. 8 for  $\text{Ta}_{50}\text{Mo}_{50}$  in the variation of the long-range order (LRO) parameter with temperature, defined as

$$\eta = \frac{1}{2c_{\text{Mo}}}(y_{\text{Mo}}^{\text{I}} - y_{\text{Mo}}^{\text{II}}) \quad (5.7)$$

where  $y_{\text{Mo}}^s$  is a direct measure of the local composition in Mo species on one of the two simple cubic sublattices ( $s=\text{I}$  or  $\text{II}$ ) that form the bcc lattice. The order parameter varies between 0 (fully disordered) to 1 (fully ordered). Note that a better agreement between CVM and CALPHAD LRO parameters could have been achieved by including information on LRO parameters in the fitting procedure in the detriment of a less accurate determination of the Gibbs energies. It is worth noting that the enthalpies of mixing calculated both ways for  $\text{Ta}_{50}\text{Mo}_{50}$  show differences that are within the accuracy of any CALPHAD-type calculations as illustrated in Fig. 8.

Another test of the validity of the fitting procedure can be made by analyzing the *ab initio* results displayed in Fig. 4 for the mixing energy with a second-order Redlich-Kister expansion. The coefficients of the expansion are (in J/mol)  ${}^0L_{\text{Ta,W}}^{\text{bcc-A2}} = -45,454$ ,  ${}^1L_{\text{Ta,W}}^{\text{bcc-A2}} = +27,961$ ,  ${}^0L_{\text{Mo,Ta}}^{\text{bcc-A2}} = -69,341$ , and  ${}^1L_{\text{Mo,Ta}}^{\text{bcc-A2}} = -19,629$ , and compare well with those given in the appendix, keeping in mind that the transcription of the *ab initio* results in a CALPHAD format has been performed between 800 and 3000 K in the case of Ta-W, and 1500 and 3000 K for Ta-Mo. The overall quality of the fit is reflected in the comparison of the phase diagrams obtained from this CALPHAD assessment, represented by a solid line in Fig. 6, and the CVM results, represented by open circles in the figure. Note that the solidus-liquidus lines are those that have been assessed within CALPHAD, based on the available experimental data [1], cf. appendix.

In the spirit of a CALPHAD assessment performed on experimental data for which the resulting Gibbs energies implicitly contained information on SRO, good agreement with experimental results can be achieved despite the fact that the configurational entropy is treated within the Bragg-Williams approximation. Because the CALPHAD methodology relies on temperature-dependent interactions, low- and high-temperature Gibbs energies can

be successfully reproduced.

To conclude this section, we have shown that the predictions from *ab initio* alloy thermodynamics can be well accounted for in a CALPHAD framework, and therefore adequately supplement existing phenomenological databases in use to study higher-order component alloys. In the next section we will show that the results obtained for the binaries re-generated in a CALPHAD format can be used to study their impact on the thermodynamics of higher-order component alloys.

## VI. THERMODYNAMIC PROPERTIES OF MO-TA-W ALLOYS

To describe the thermodynamic properties of the ternary alloy within *ab initio*, we will assume that the EPIs obtained for the three binaries are not altered by the presence of a third element. This translates in the neglect of specific ternary interaction parameters in the definition of the excess Gibbs energy, a common assumption made when describing higher-order component alloys within CALPHAD. In both cases, the excess Gibbs energy is given by a Muggianu-like expression [43], see Eq.(5.2). In existing thermodynamic databases such as SSOL provided by SGTE [41], the three binary subsystems are treated as ideal solid solution (i.e., no excess Gibbs energies), and therefore the solidus-liquidus lines that separate the liquid from the bcc solid solution is the only feature that characterizes isothermal sections of the ternary phase diagram between the melting points of Mo (2890 K) and W (3680 K), as shown in Fig. 9. With the CALPHAD assessment of the *ab initio* data presented in the previous section the high-temperature isothermal sections are only slightly modified, as shown in the figure, because of the fitting procedure that guarantees compatibility between the Gibbs energies of the bcc-A2 solid solution and the liquid phase. On the other hand, as expected, the two phase diagrams in the solid phase differ noticeably. The CALPHAD phase diagram obtained with the SSOL thermodynamic database only displays a region of bcc solid solution whereas, below about 1800 K, the *ab initio*-CALPHAD one shows in Fig. 10a a region of stability of B2 ordered phase that connects the two binaries Ta-W and

Ta-Mo, with a maximum temperature associated with  $c_W=0$ . It is worth mentioning that because of the assumption made on the description of the ternary system, we may miss some enhancement effect due to ternary addition that could lead to a higher order-disorder temperature at fixed and non-zero Mo, Ta, and W mole fractions.

To check how well the expression for the Gibbs energy is extended to the ternary case, an *ab initio* study of the ternary system has been carried out within the approximation alluded to in the introduction of this section. Note that the extension of the CVM to multi-component systems [51] has been applied to only a few ternary systems, *e.g.* cf. Refs. [52–54]. In the present case the irregular tetrahedron approximation of the CVM has still been considered for the Mo-Ta-W system (in what follows the irregular tetrahedron will be described by its 4 first-neighbor pairs and 2 second-neighbor ones referred to by  $\{ik, il, jk, jl\}$  and  $\{ij, kl\}$ ). The internal energy of the bcc-based system per lattice site is expressed as

$$E = 6 \sum_{ijkl} z_{ijkl} \epsilon_{ijkl} \quad (6.1)$$

where  $\epsilon_{ijkl}$  is the energy of the tetrahedron in the configuration  $\{ijkl\}$  with probability  $z_{ijkl}$ . This energy can be expressed as a function of pairwise interaction energies according to

$$\epsilon_{ijkl} = \frac{1}{6}(\epsilon_{ik}^{(1)} + \epsilon_{il}^{(1)} + \epsilon_{jk}^{(1)} + \epsilon_{jl}^{(1)}) + \frac{1}{4}(\epsilon_{ij}^{(2)} + \epsilon_{kl}^{(2)}) \quad (6.2)$$

where the constants 1/6 and 1/4 account for the fact that the first and second neighbors pairs are common to 6 and 4 tetrahedra, respectively. With the expression (6.1) for the internal energy of an alloy, the energy parameters for the binary subsystems have been redefined in such a way that they give the same ordering energies as those obtained within the GPM as follows [53]

$$\begin{aligned} \epsilon_{AAAB} &= \frac{1}{6} \Delta E_{A_3B}^{D0_3} \\ \epsilon_{AABB} &= \frac{1}{6} \Delta E_{AB}^{B2} \\ \epsilon_{ABAB} &= \frac{1}{6} \Delta E_{AB}^{B32} \end{aligned} \quad (6.3)$$

where the sequence  $\{ijkl\}, (i, j = A, B)$  describes the occupation of the four sites of a tetrahedron as discussed above. The ordering energies on the right-hand side of Eqs. (6.3)

are given within the GPM by Eq.(3.2). Note that this method is equivalent to defining a Hamiltonian as proposed in the Connolly-Williams method [55], and gives phase diagram results (dashed line) that are almost undistinguishable from those obtained in section IV (open circles), as shown in Fig. 6.

In the ternary case, two methods have been considered to estimate the pairwise interaction energies [53], and both neglect ternary interaction parameters. In the first method we assume that these energies are given by

$$\begin{aligned}\epsilon_{AABC} &= \frac{1}{2}\epsilon_{AABB} + \frac{1}{2}\epsilon_{AACC} + \frac{1}{2}\epsilon_{BCBC} - \frac{1}{4}\epsilon_{BBCC} \\ \epsilon_{ABAC} &= \frac{1}{2}\epsilon_{ABAB} + \frac{1}{2}\epsilon_{ACAC} + \frac{1}{4}\epsilon_{BBCC}\end{aligned}\tag{6.4}$$

with the energies of the other configurations obtained by permutation of the species. In the second method, the pairwise interaction energies have been defined in such a way that they reproduce the energies of ordered configurations specifically found in ternary alloys, such as the  $L2_1$  and  $F\bar{4}3m$  ordered states given at the composition  $A_2BC$  (cf. Ref. [53] for a description of these superstructures). For these two states, the ordering energies are given by

$$\begin{aligned}\Delta E_{\text{ord}}^{L2_1, A_2BC} &= -\frac{1}{2}(V_1^{AB} + V_1^{AC}) + \frac{1}{4}V_1^{BC} + \frac{3}{8}(V_2^{AB} + V_2^{AC}) - \frac{9}{16}V_2^{BC} \\ \Delta E_{\text{ord}}^{F\bar{4}3m, A_2BC} &= -\frac{3}{8}(V_2^{AB} + V_2^{AC}) - \frac{1}{4}V_1^{BC} + \frac{3}{16}V_2^{BC}\end{aligned}\tag{6.5}$$

with corresponding expressions for states at the compositions  $B_2AC$  and  $C_2AB$  by permutation of A, B, and C in Eq. (6.5). In these expressions, the  $V_s^{IJ}$  are in principle those EPIs estimated from GPM calculations for ternary alloys. However to compare the *ab initio* results to those obtained within the *ab initio*-CALPHAD treatment of ternary alloys, the EPIs have been evaluated from the data available for the binary subsystems only. Hence, at the composition  $A_2BC$ , the  $V_s^{AB}$  and  $V_s^{AC}$  ( $s = 1, 2$ ) are taken at the composition  $x_A = 3/8$  for the alloys A-B and A-C whereas the  $V_1^{BC}$  is taken at the composition  $x_B = 1/2$  for the alloy B-C.

Note that the first method is more in line with the calculations that can be performed within CALPHAD, as shown by comparing the solid-phase portion of the phase diagrams shown in Figs. 10b (first method) and 10c (second method) with the one obtained from *ab initio*-CALPHAD calculations presented in Fig. 10a. The CVM improvement of the ideal Gibbs energy (or configurational entropy) over the Bragg-Williams estimation is still noticeable although the impact of SRO in ternary alloys becomes less pronounced than in the binary case. To conclude this section, we have shown that the information collected from *ab initio* can be used to study the stability properties of ternary alloys, and make use of powerful commercial software to easily compute their phase diagrams. The comparison between a full *ab initio* thermodynamic treatment and the *ab initio*-CALPHAD results indicate that the Bragg-Williams approximation for the configurational entropy is better justified for higher-order component alloys than it was for binaries. This later point adds to the assumption that complex multi-component systems can be studied from the knowledge of binaries (and in some instances ternary systems) without having to include additional information than the one gathered for the binary subsystems.

## VII. CONCLUSIONS

Detailed calculations were carried out on electronic structure and equilibrium properties of Ta-W, Ta-Mo, and Mo-W alloys using the TB-LMTO formulation of the coherent potential approximation. The GPM was used to predict ordering tendencies and related thermodynamic information across the concentration range of these alloys. Temperature effects were accounted for within the generalized mean-field approach on which the CVM is based. We predict that Ta-W and Ta-Mo alloys should exhibit a tendency towards order with a B2 superstructure in a broad range of alloy composition. This should not come as a surprise since experimentally there were indications that these two alloy systems should not follow an ideal law of mixing. This result is also consistent with the behavior of quantities related to ordering trends in alloys, such as the negative departure from Vegard's law of the

equilibrium lattice constant and the negative departure from Raoult’s law of the activity of each alloy species, as a function of composition.

Although a solid phase part of the phase diagram of Ta-Mo and Ta-W is predicted at low temperature, relatively to the location of the solidus-liquidus line, the second-order nature of the transition from B2 to the disordered state can be used advantageously to identify B2 short-range order. Diffuse scattering experiments should provide a quantitative measure of the ordering strength in these alloys, and confirm or challenge these predictions. In contrast to the two previous alloys, we find that Mo-W should behave like an ideal solid solution if one neglects the slight tendency towards phase separation that should occur at extremely low temperatures.

In the second part of this study we have shown that the results of *ab initio* thermodynamics can be cast in a CALPHAD formalism for subsequent prediction of isothermal sections of ternary phase diagrams. Short-range order effects that indicate departure from ideal solid solution behavior are accounted for in an approximate way by assessing the *ab initio* results in the same way experimental phase diagram information are, hence providing a robust and yet simple scheme that is consistent with standard assessment of multi-component alloy phase diagrams. In the case of the Mo-Ta-W phase diagram, *ab initio* alloy thermodynamics of the binary subsystems has been transcribed in a CALPHAD format to generate isothermal sections of the ternary phase diagram. We have shown that the results compare favorably to those directly obtained by performing CVM calculations for the ternary system. This observation indicates that SRO effects become negligible, thus validating a single-site Bragg-Williams statistical treatment of chemical order for higher-order component alloys. The phenomenological thermo-chemical database has been supplemented with *ab initio* information, and predictions have been made on the existence, at low temperatures, of a B2 ordered phase in a broad range of alloy composition in the ternary Mo-Ta-W system. With the present interface being validated, one can envision that the reverse path from CALPHAD to *ab initio* may be used as a tool to challenge *ab initio* predictions on binary systems from experimental information gathered on ternary or higher-order component

alloys, a knowledge that was until now ignored.

## VIII. ACKNOWLEDGMENTS

This work performed under the auspices of the U.S. Department of Energy by the University of California Lawrence Livermore National Laboratory under contract No. W-7405-ENG-48. The work of V. D. and J. K. was carried out within the project AV0Z1-010-914 of the Academy of Sciences of the Czech Republic, and supported by the Grant Agency of the Academy of Sciences of the Czech Republic (Project A1010203).

## IX. APPENDIX

Solution and compound phase parameters for the three binaries of the Mo-Ta-W system (Temperature T in K, and energy in J/mol), as obtained from CALPHAD assessments performed on the thermodynamic results from *ab initio*. Parameters not indicated here are implicitly set to zero. Notations are explained in the text.

Liquid: 1-sublattice model (Mo,Ta,W)<sub>1</sub>

$${}^0L_{\text{Ta,W}}^{\text{liq}} = A_0 - 4,000$$

$${}^1L_{\text{Ta,W}}^{\text{liq}} = A_1$$

$${}^0L_{\text{Mo,Ta}}^{\text{liq}} = B_0 - 3,000$$

$${}^1L_{\text{Mo,Ta}}^{\text{liq}} = B_1$$

bcc-A<sub>2</sub>: 1-sublattice model (Mo,Ta,W)<sub>1</sub>

$${}^0L_{\text{Ta,W}}^{\text{bcc-A2}} = A_0$$

$${}^1L_{\text{Ta,W}}^{\text{bcc-A2}} = A_1$$

$${}^0L_{\text{Mo,Ta}}^{\text{bcc-A2}} = B_0$$

$${}^1L_{\text{Mo,Ta}}^{\text{bcc-A2}} = B_1$$

$${}^0L_{\text{Mo,W}}^{\text{bcc-A2}} = +2,000$$



bcc-B<sub>2</sub>: 2-sublattice model (Mo,Ta,W)<sub>0.5</sub>(Mo,Ta,W)<sub>0.5</sub> (with  $N_I = 0.5$  and  $N_{II} = 0.5$ )

$$\Delta G_{\text{Ta:W}}^{\text{bcc-B2}} = \Delta G_{\text{W:Ta}}^{\text{bcc-B2}} = C_0$$

$$\Delta G_{\text{Mo:Ta}}^{\text{bcc-B2}} = \Delta G_{\text{Ta:Mo}}^{\text{bcc-B2}} = D_0$$

$${}^0L_{\text{Ta:Ta,W}}^{\text{bcc-B2}} = {}^0L_{\text{Ta,W:Ta}}^{\text{bcc-B2}} = C_1$$

$${}^0L_{\text{Ta,W:W}}^{\text{bcc-B2}} = {}^0L_{\text{W:Ta,W}}^{\text{bcc-B2}} = -C_1$$

$${}^0L_{\text{Mo:Mo,Ta}}^{\text{bcc-B2}} = {}^0L_{\text{Mo,Ta:Mo}}^{\text{bcc-B2}} = D_1$$

$${}^0L_{\text{Mo,Ta:Ta}}^{\text{bcc-B2}} = {}^0L_{\text{Ta:Mo,Ta}}^{\text{bcc-B2}} = -D_1$$

with

$$A_0 = -54,661 + 7.012 T - 1.2958 \cdot 10^{-3} T^2$$

$$A_1 = +29,646 - 0.467 T$$

$$B_0 = -76,019 + 2.721 T - 0.0426 \cdot 10^{-3} T^2 - 8.23845 \cdot 10^{-8} T^3$$

$$B_1 = -18,025 - 4.164 T + 2.1399 \cdot 10^{-3} T^2 - 3.24184 \cdot 10^{-8} T^3$$

$$C_0 = -3,788 - 3.864 T - 0.6479 \cdot 10^{-3} T^2$$

$$D_0 = -9,000 - 3.085 T - 0.0213 \cdot 10^{-3} T^2$$

$$C_1 = -838 + 2.697 T$$

$$D_1 = +1,778 - 3.479 T + 1.0700 \cdot 10^{-3} T^2$$

## REFERENCES

- [1] *Binary Alloy Phase Diagrams*, T. B. Massalski ed. (ASM International, Materials Park, OH, 1990), vols. **1** to **3**.
- [2] R. Krishnan, S. P. Garg, and N. Krishnamurthy, *J. Alloy Phase Diag.* **2**, 205 (1986).
- [3] R. Predmore and R. J. Arsenault, *Script. Metall.* **4** 213 (1970).
- [4] G. A. Geach and D. Summers-Smith, *J. of the Inst. of Met.* **80**, 143 (1951-1952).
- [5] L. I. van Torne and G. Thomas, *Acta. Metall.* **14**, 621 (1966).
- [6] R. Krishnan, S. P. Garg, and N. Krishnamurthy, *J. of Alloy Phase Diag.* **3**, 1 (1987).
- [7] S. C. Singhal and W. L. Worrell, *Met. Trans.* **4**, 895 (1973).
- [8] P. E. A. Turchi, A. Gonis, V. Drchal, and J. Kudrnovský, *Phys. Rev. B* **64**, 085112 (2001).
- [9] F. Ducastelle and F. Gautier, *J. Phys. F: Met. Phys.* **6**, 2039 (1976).
- [10] F. Ducastelle, *Order and Phase Stability in Alloys*, ed. by F. R. de Boer and D. G. Pettifor (North-Holland, Amsterdam, 1991), *Cohesion and Structure* series, vol. **3**.
- [11] P. E. A. Turchi, in *Intermetallic Compounds: Principles and Practice*, ed. by J. H. Westbrook and R. L. Fleischer (John Wiley & Sons, Ltd., New York, 1995), vol. **1**, Chap. 2, pp. 21-54.
- [12] I. Turek, V. Drchal, J. Kudrnovský, M. Šob, and P. Weinberger, *Electronic Structure of Disordered Alloys, Surfaces and Interfaces* (Kluwer, Boston-London-Dordrecht, 1997).
- [13] J. S. Faulkner, in *Progress in Materials Science*, ed. by J. W. Christian, P. Hassen and T. B. Massalski (Pergamon Press, New York, 1982), vol. **27**, No. 1 and No. 2; and references cited therein.
- [14] R. Kikuchi, *Phys. Rev.* **81**, 988 (1951).

- [15] O. Redlich and A. Kister, *Ind. Eng. Chem.* **40**, 345 (1948).
- [16] L. Kaufman, P. E. A. Turchi, W. Huang, and Zi-Kui Liu, *CALPHAD* **25**, 419 (2001).
- [17] L. Kaufman and H. Bernstein, *Computer Calculation of Phase Diagrams with Special Reference to Refractory Metals* (Academic Press, New York, 1970).
- [18] *CALPHAD and Alloy Thermodynamics*, ed. by P. E. A. Turchi, A. Gonis, and R. D. Shull (TMS, Warrendale, 2002).
- [19] N. Saunders and A. P. Miodownik, *CALPHAD - Calculation of Phase Diagrams: A Comprehensive Guide*, Pergamon Materials series ed. by R. W. Cahn, vol. **1** (Elsevier, Oxford, 1998).
- [20] G. Grimvall, *Ber. Bunsenges. Phys. Chem.* **102**, 1083 (1998).
- [21] D. M. Ceperley and B. J. Alder, *Phys. Rev. Lett.* **45**, 566 (1980).
- [22] J. P. Perdew and A. Zunger, *Phys. Rev. B* **23**, 5048 (1981).
- [23] H. L. Skriver, *The LMTO Method*, Springer series in Solid-State Sciences, vol. **41** (Springer-Verlag, Heidelberg, 1983); O. K. Andersen, O. Jepsen, and D. Glötzl, in *Highlights of Condensed Matter Theory*, ed. by F. Bassani, F. Fumi, and M. P. Tosi (North-Holland, Amsterdam, 1985), p. 59.
- [24] U. von Barth and L. Hedin, *J. Phys. C: Condensed Matter* **5**, 1629 (1972).
- [25] C. Colinet, A. Bessoud, and A. Pasturel, *J. Phys. F: Met. Phys.* **18**, 903 (1988).
- [26] D. G. Pettifor, in *Physical Metallurgy*, ed. by R. W. Cahn and P. Hassen (North-Holland, Amsterdam, 1983), chapt. 3.
- [27] R. Hawkins, M. O. Robbins, and J. M. Sanchez, *Phys. Rev. B* **33**, 4782 (1986).
- [28] A. Finel and F. Ducastelle, in *Phase Transformations in Solids*, ed. by T. Tsakalakos (North-Holland, Amsterdam, 1984), p. 293.

- [29] A. Finel, D. Gratias, and R. Portier, in *L'Ordre et le Désordre dans les Matériaux* (Les Editions de Physique, Les Ulis, 1984), p. 9.
- [30] A. Finel, Thèse de Doctorat d'Etat es Sciences Physiques, University Paris VI, France, unpublished (1987); and Technical Report ONERA 1987-3.
- [31] S. M. Allen and J. W. Cahn, *Acta Metall.* **20**, 423 (1972).
- [32] G. Kresse and J. Furthmüller, *Comput. Mater. Sci.*, **6**, 15 (1996).
- [33] V. Blum and A. Zunger, *Phys. Rev. B* **69**, 020103 (2004).
- [34] C. Sigli, M. Kosugi, and J. M. Sanchez, *Phys. Rev. Lett.* **57**, 253 (1986).
- [35] N. S. Golosov and A. M. Tolstik, *J. Phys. Chem. Sol.* **36**, 899, 903 (1975).
- [36] V. L. Moruzzi, J. F. Janak, and K. Schwarz, *Phys. Rev.* **37**, 790 (1988).
- [37] C. Bichara and G. Inden, in *Statics and Dynamics of Alloy Phase Transformations*, NATO-ASI Series, series B: Physics, vol. **319**, ed. by P. E. A. Turchi and A. Gonis (Plenum Press, New York, 1994), p. 541.
- [38] L. Kaufman and H. Bernstein, *Computer Calculation of Phase Diagrams with Special Reference to Refractory Metals* (Academic Press, New York, 1970).
- [39] MRS Bulletin, Vol. **24**, No. 4, pp 18-49 (April 1999).
- [40] *CALPHAD and Alloy Thermodynamics*, ed. by P. E. A. Turchi, A. Gonis, and R. D. Shull (TMS Publication, Warrendale, PA, 2002); and references therein.
- [41] I. Ansara and B. Sundman, *The Scientific Group Thermodata Europe*, P. S. Glaeser ed., Computer Handling and Dissemination of Data (Elsevier Science Pub. Co., 1987).
- [42] A. Dinsdale, *CALPHAD* **15**, 317 (1991).
- [43] Y. M. Muggianu, M. Gambino, and J. P. Bros, *J. Chem. Phys.* **22**, 83 (1975).

- [44] O. Redlich and A. Kister, *Ind. Eng. Chem.* **40**, 345 (1948).
- [45] B. Sundman and J. Agren, *J. Phys. Chem. Sol.* **42**, 297 (1981).
- [46] J. O. Andersson, A. F. Guillermet, M. Hillert, B. Jansson, and B. Sundman, *Act. Metall.* **34**, 1986 (1986).
- [47] I. Ansara, N. Dupin, and B. Sundman, *CALPHAD* **21**, 535 (1997).
- [48] B. Jansson, Trita-Mac-0234, Royal Institute of Technology, Stockholm, Sweden (1984).
- [49] B. Sundman, B. Jansson, and J.-O. Andersson, *CALPHAD* **9**, 153 (1985).
- [50] The results of the fitting procedure for Ta-W that are reported in the appendix have been corrected for a few typographical errors that appear in Ref. [16].
- [51] H. Ackermann, G. Inden, and R. Kikuchi, *Acta Metall. Mater.* **37**, 1 (1989).
- [52] G. Rubin and A. Finel, *J. Phys.: Condens. Matter* **7**, 3139 (1995).
- [53] V. Chaumat, C. Colinet, and F. Moret, *J. of Phase Equil.* **20**, 389 (1999).
- [54] C. Colinet, Ref. [40], pp. 21-52; and references therein.
- [55] J. W. D. Connolly and A. R. Williams, *Phys. Rev. B* **27**, 5169 (1983).

# TABLES

TABLE I. Equilibrium properties, *i.e.*, lattice constant (in Å), bulk modulus (in GPa), and when applicable formation energy of the ordered B2 phase (in kJ/mol), of bcc-based pure Ta, Mo, and W, and of the B2 ordered phase of TaW and TaMo. Methods 1 and 2 correspond to LMTO-ASA, and TB-LMTO-ASA in the case of the pure species or TB-LMTO-CPA-GPM in the case of the ordered B2 phase of TaW and TaMo, respectively.

Property	Method	Pure Ta	Pure Mo	Pure W	Ordered B2 TaW	Ordered B2 TaMo
Lattice Constant	Experiment	3.3031	3.1472	3.1652	-	-
(in Å)	Method 1	3.3098	3.1781	3.1934	3.2421	-
	Method 2	3.2766	3.1738	3.1802	3.2203	3.2139
Bulk Modulus	Experiment	196.1	262.6	310.4	-	-
(in GPa)	Method 1	206.4	273.1	314.0	255.8	-
	Method 2	215.3	291.9	337.3	276.8	226.7
$\Delta E_{\text{form}}^{\text{B2}}$	Method 1	-	-	-	-10.5	-
(in kJ/mol)	Method 2	-	-	-	-17.0	-26.5

## FIGURES

FIG. 1. Density of states of bcc-based pure Ta, Mo, and W (left panels), and of  $\text{Ta}_{50}\text{W}_{50}$ ,  $\text{Ta}_{50}\text{Mo}_{50}$ , and  $\text{Mo}_{50}\text{W}_{50}$  disordered alloys (right panels) as a function of energy, as obtained from TB-LMTO-CPA. The Fermi energy  $E_F$  is indicated by a vertical line and taken as zero of energy. In the alloy case, the solid line indicates the total density of states, whereas the dotted and dashed line refer to the partial densities of states of Ta (Ta, Mo) and W (Mo, W).

FIG. 2. Variation of the bcc lattice constant  $a^{\text{eq}}$  (in Å) of the chemically random alloys Ta-W (solid circle), Ta-Mo (open circle), and Mo-W (square) (top), and of the departure from Vegard's law,  $\delta a^{\text{eq}}$  (in Å) (bottom) with alloy composition. The dashed line corresponds to the theoretical results and the solid line to the experimental data from Ref. [6] and [2] for Ta-W and Ta-Mo, respectively.

FIG. 3. Variation of the bulk modulus (in GPa) of the bcc-based chemically random Ta-W (solid circle), Ta-Mo (open circle), and Mo-W (square) alloys with composition. The solid circles indicate the experimental value of the endpoints.

FIG. 4. Variation of the mixing energy  $\Delta E_{\text{mix}}$  (in kJ/mol) of the bcc-based chemically random Ta-W (solid circle), Ta-Mo (open circle), and Mo-W (square) alloys with composition.

FIG. 5. First (solid line) and second (dashed line) effective pair interactions (EPIs)  $V_1$  and  $V_2$  (in kJ/mol) as functions of composition for bcc-based Ta-W (solid circle), Ta-Mo (open circle), and Mo-W (square) alloys, as obtained from TB-LMTO-CPA-GPM.

FIG. 6. Predicted bcc-based Ta-W (a) and Ta-Mo (b) phase diagrams, as obtained from the tetrahedron approximation of the CVM (open circles) and from the CALPHAD data summarized in the appendix (solid lines). The CVM results based on the Hamiltonian described in section VI are represented by a dashed line.

FIG. 7. Molar Gibbs energy (a) and molar enthalpy (b) (in kJ/mol) of Mo-Ta alloy as functions of Ta composition and at various temperatures. The points are derived from the *ab initio* method (see text) whereas the curves are obtained from the *ab initio*-CALPHAD approach.

FIG. 8. Enthalpy of mixing (in kJ/mol) and order parameter of  $\text{Mo}_{50}\text{Ta}_{50}$  alloy as functions of temperature (in K) obtained from CVM (solid lines) and *ab initio*-CALPHAD modeling (dotted lines).

FIG. 9. Isothermal sections of the phase diagram of Mo-Ta-W as obtained from CALPHAD (left panels) and from *ab initio*-CALPHAD (right panels) calculations performed at 3000, 3200, and 3400 K (from top to bottom).

FIG. 10. Solid-state portion of the Phase diagram of Mo-Ta-W obtained from *ab initio*-CALPHAD (a), and from *ab initio*-CVM with method 1 (b) and method 2 (c); see text for details.



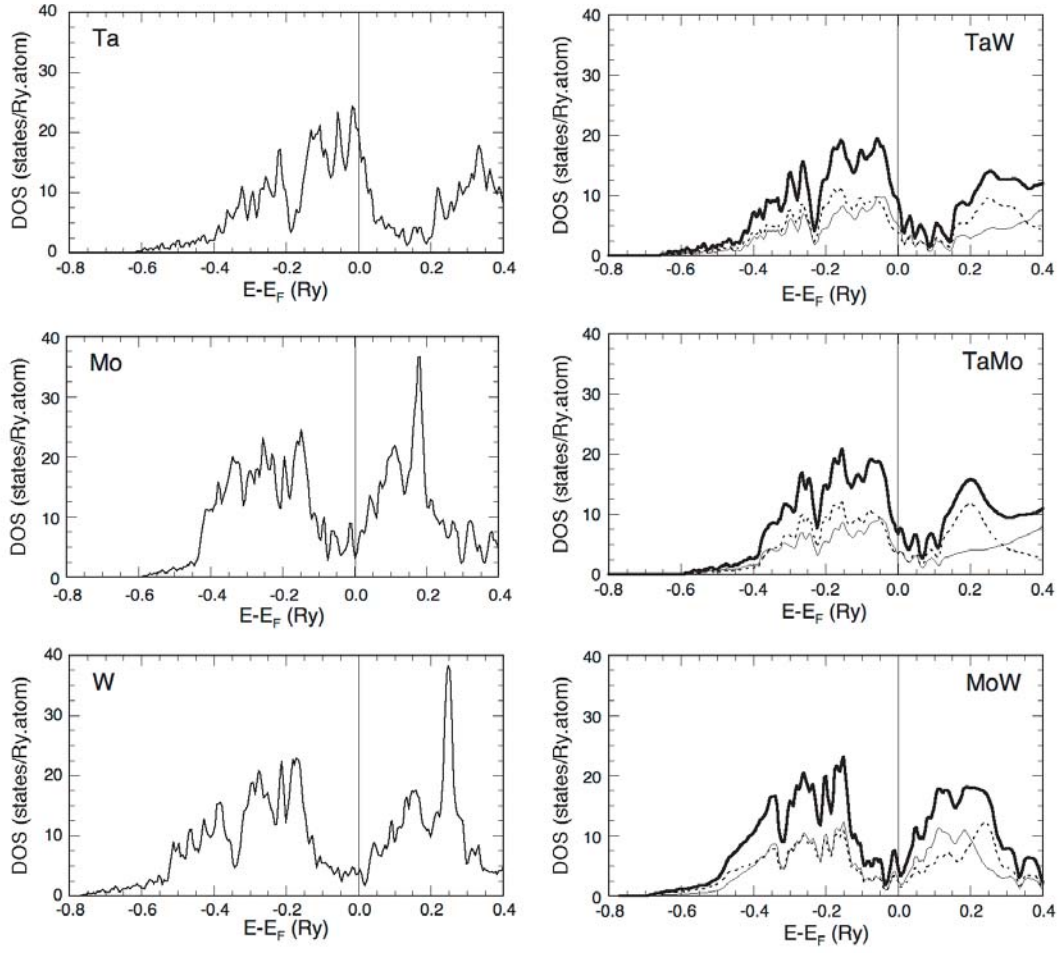


FIG. 1. Turchi et al.

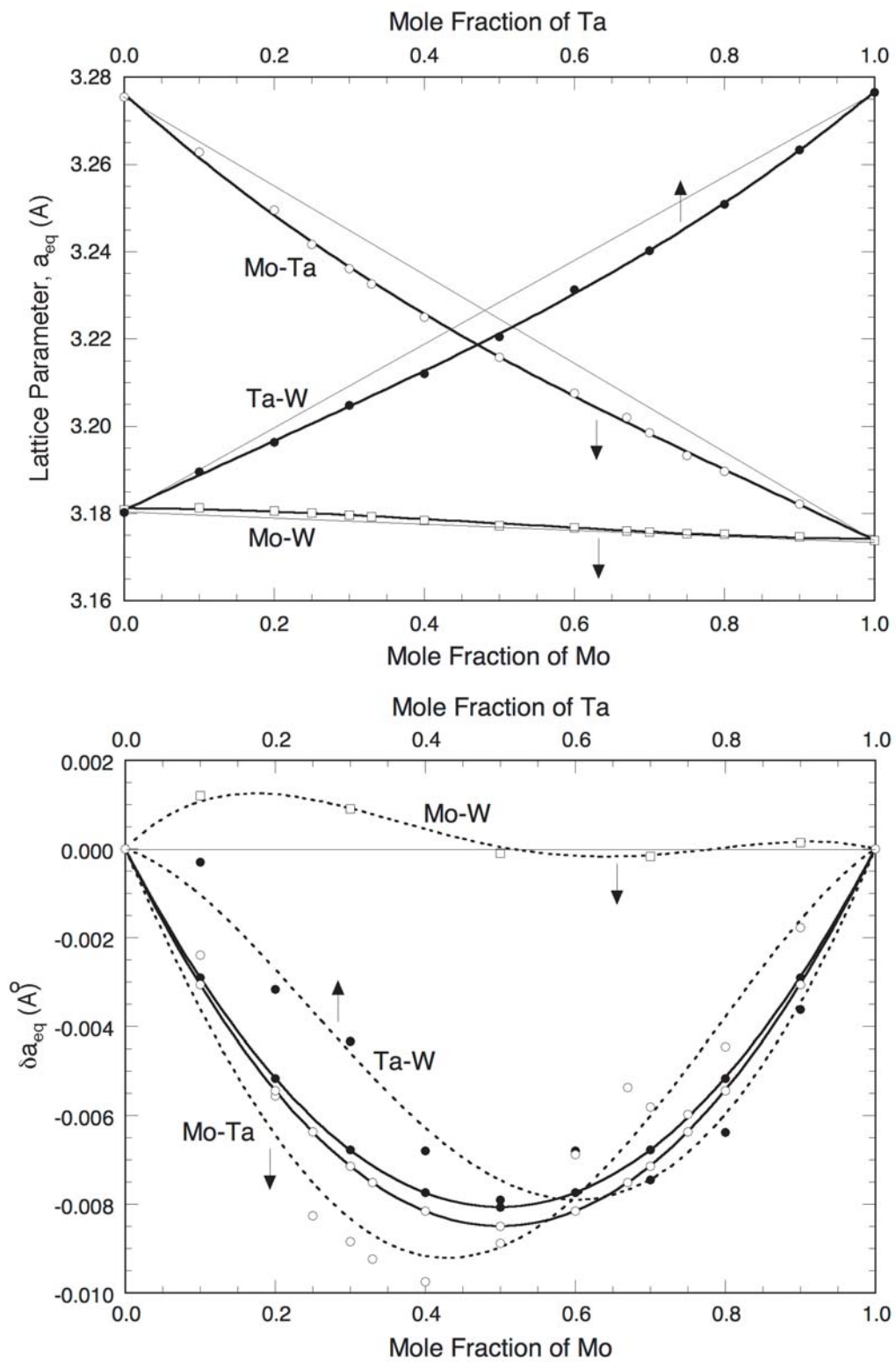


FIG. 2. Turchi et al.

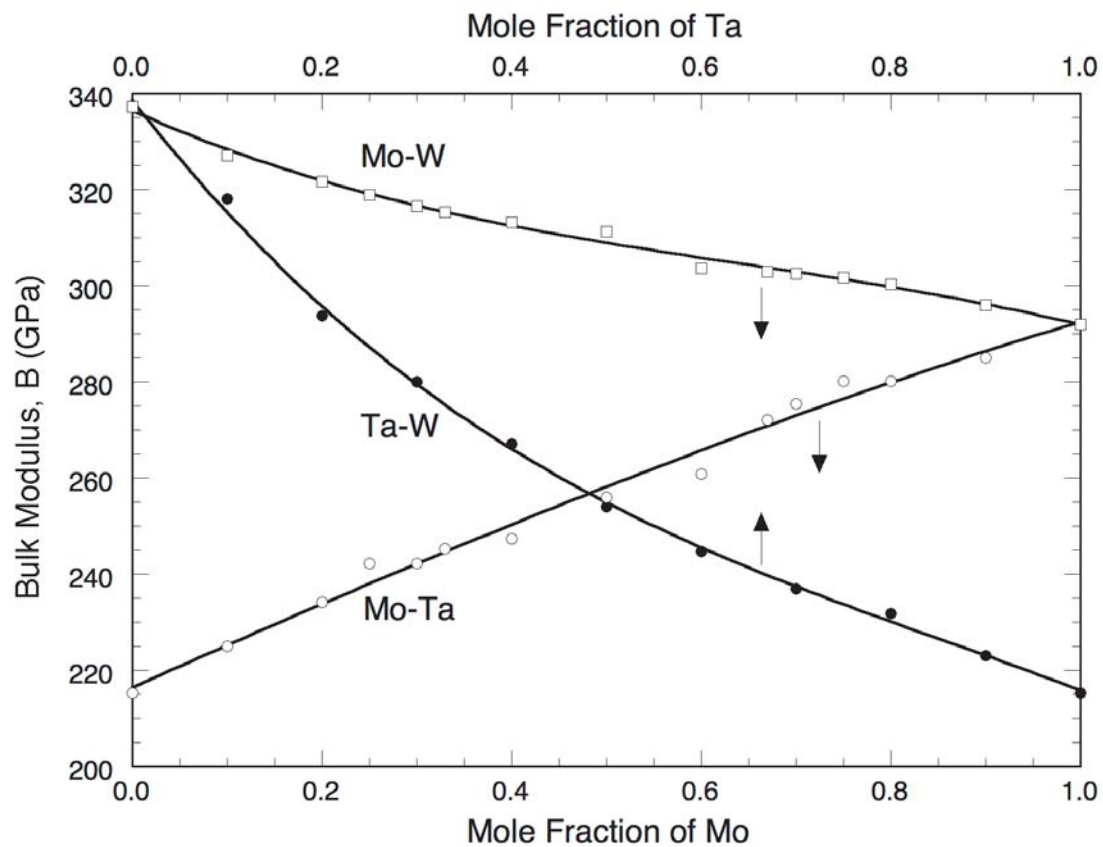


FIG. 3. Turchi et al.

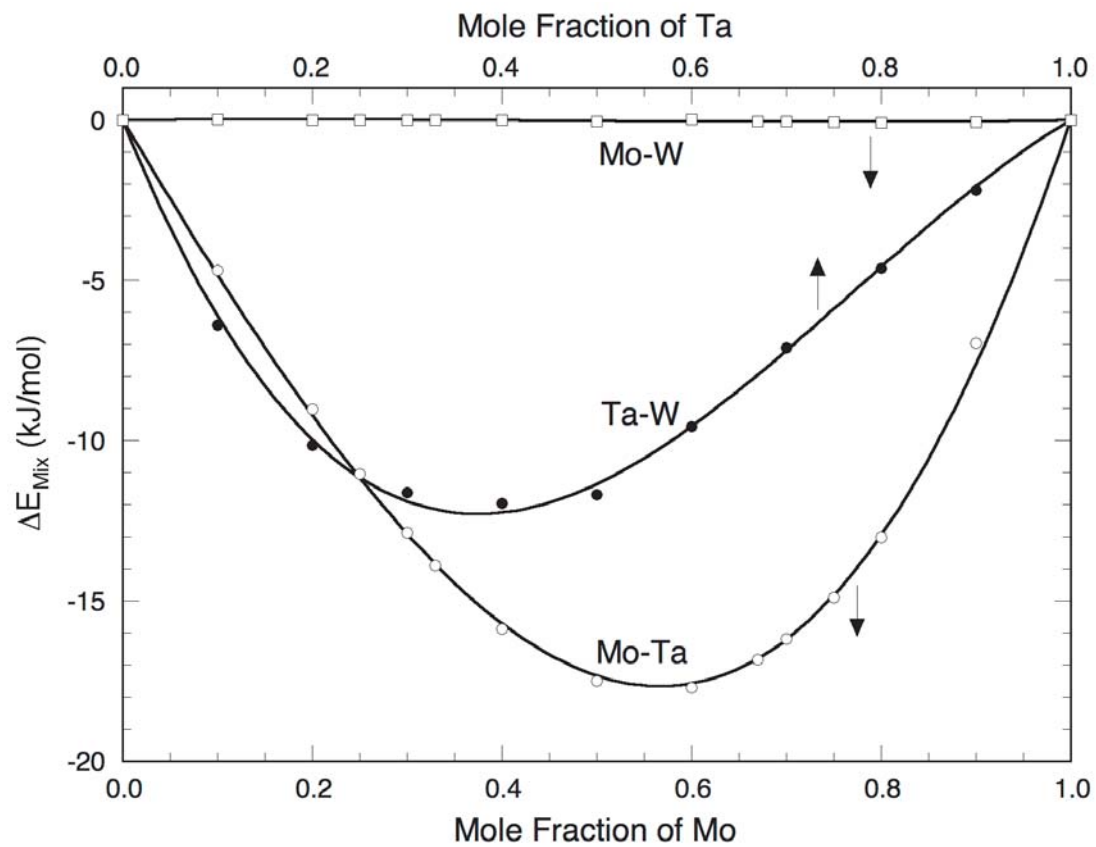


FIG. 4. Turchi et al.

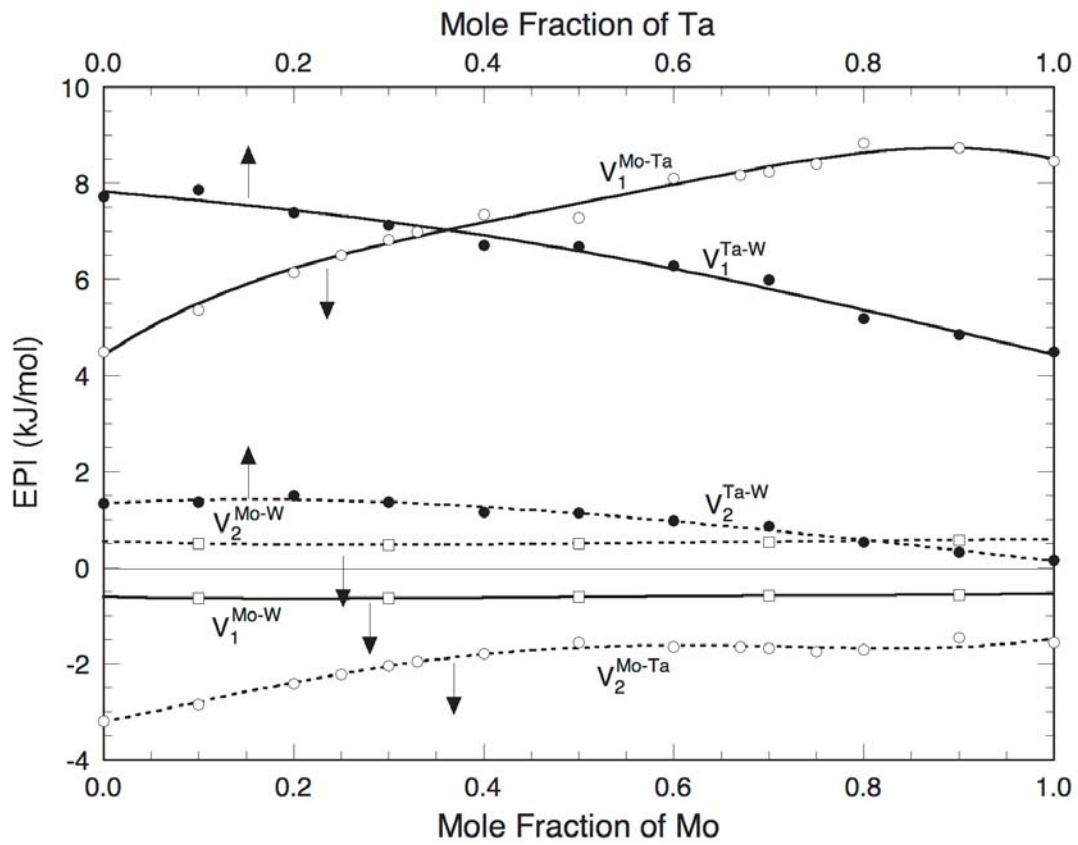


FIG. 5. Turchi et al.

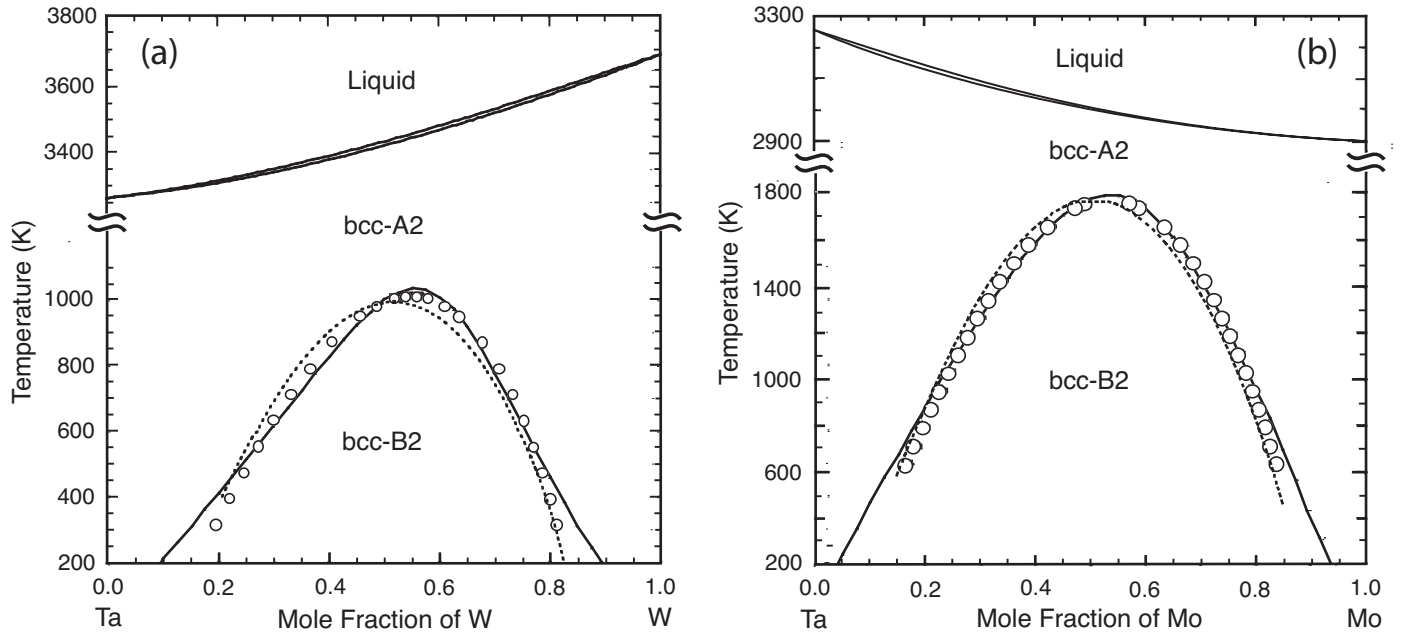


FIG. 6. Turchi et al.

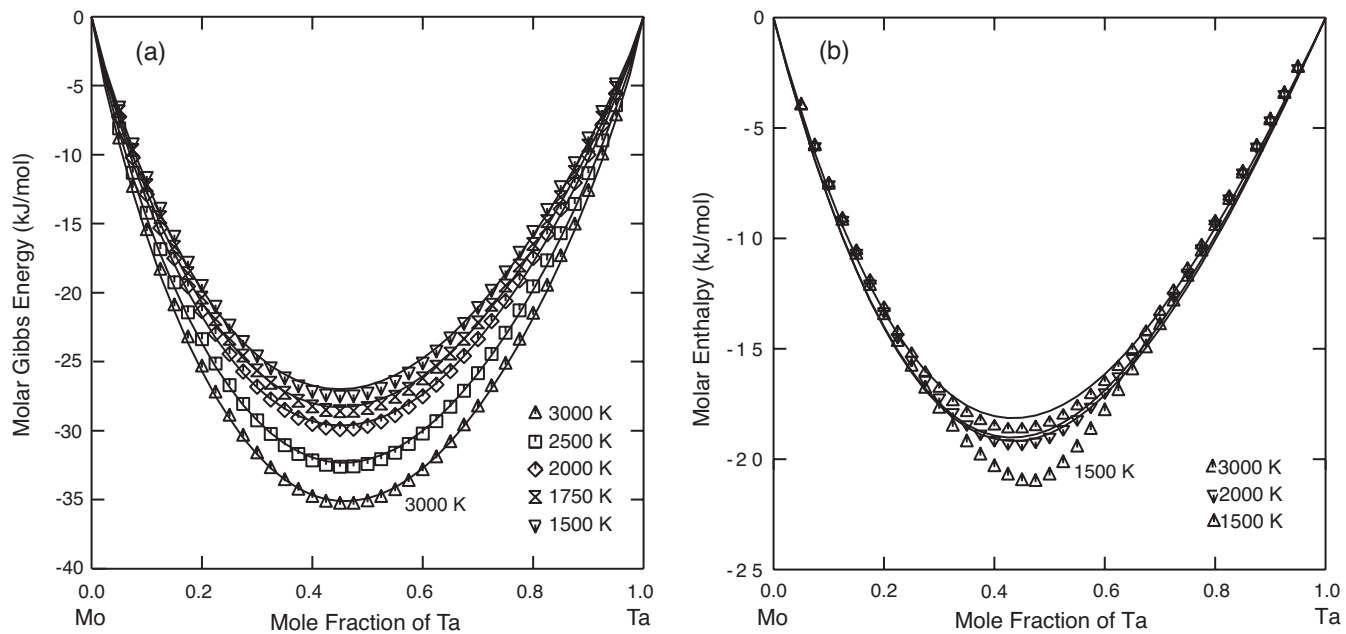


FIG. 7. Turchi et al.

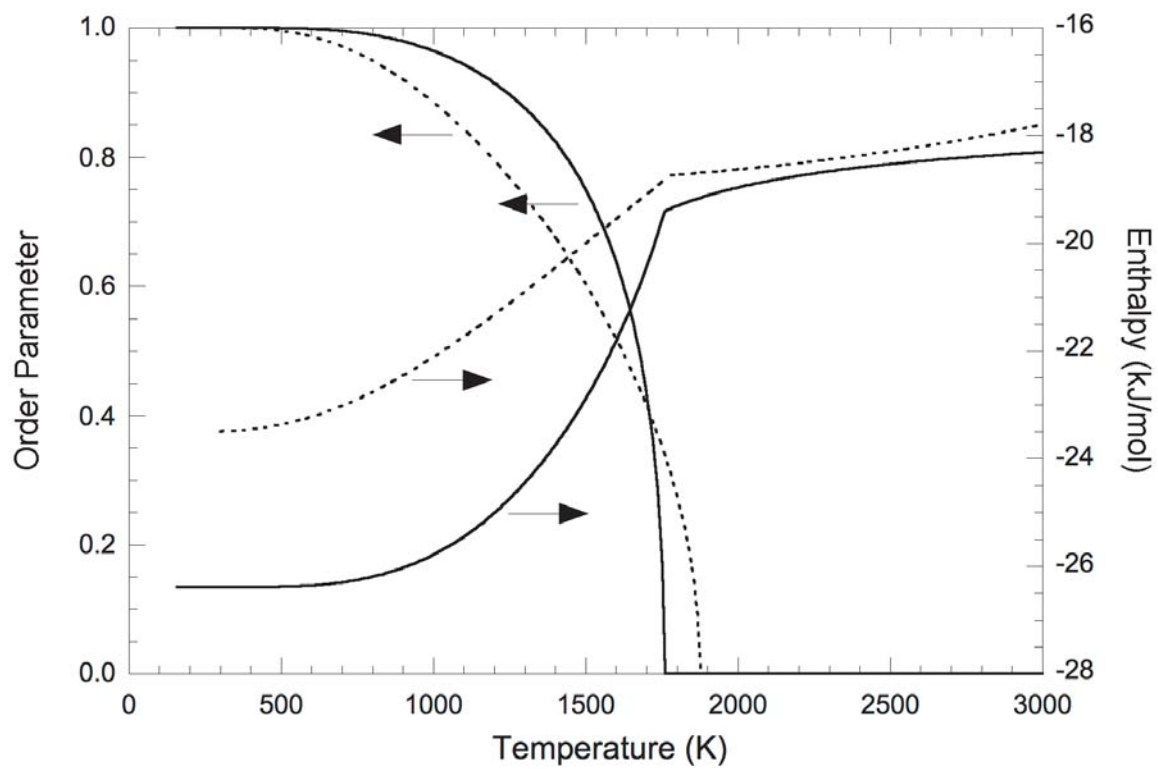


FIG. 8. Turchi et al.



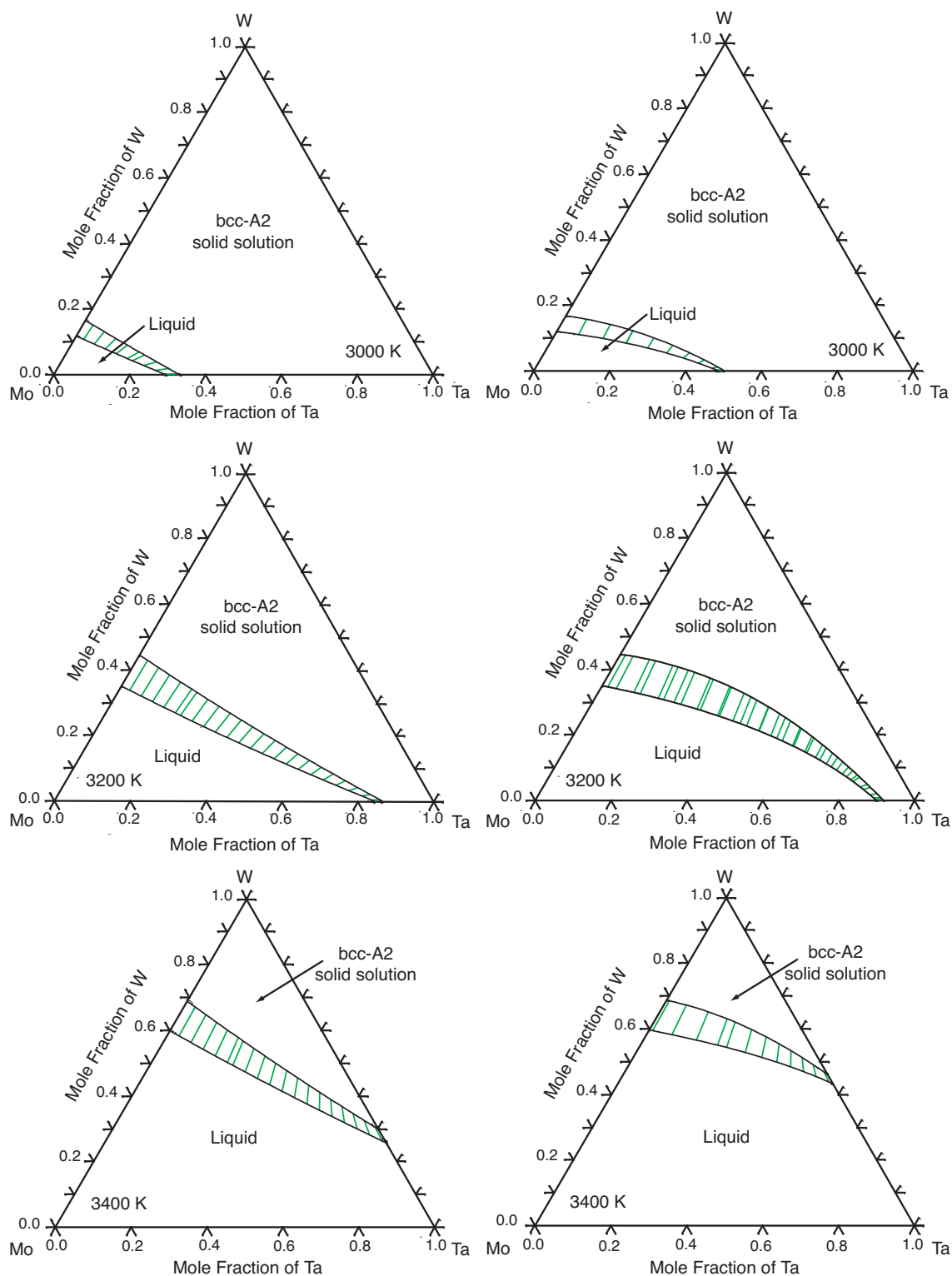


FIG. 9. Turchi et al.

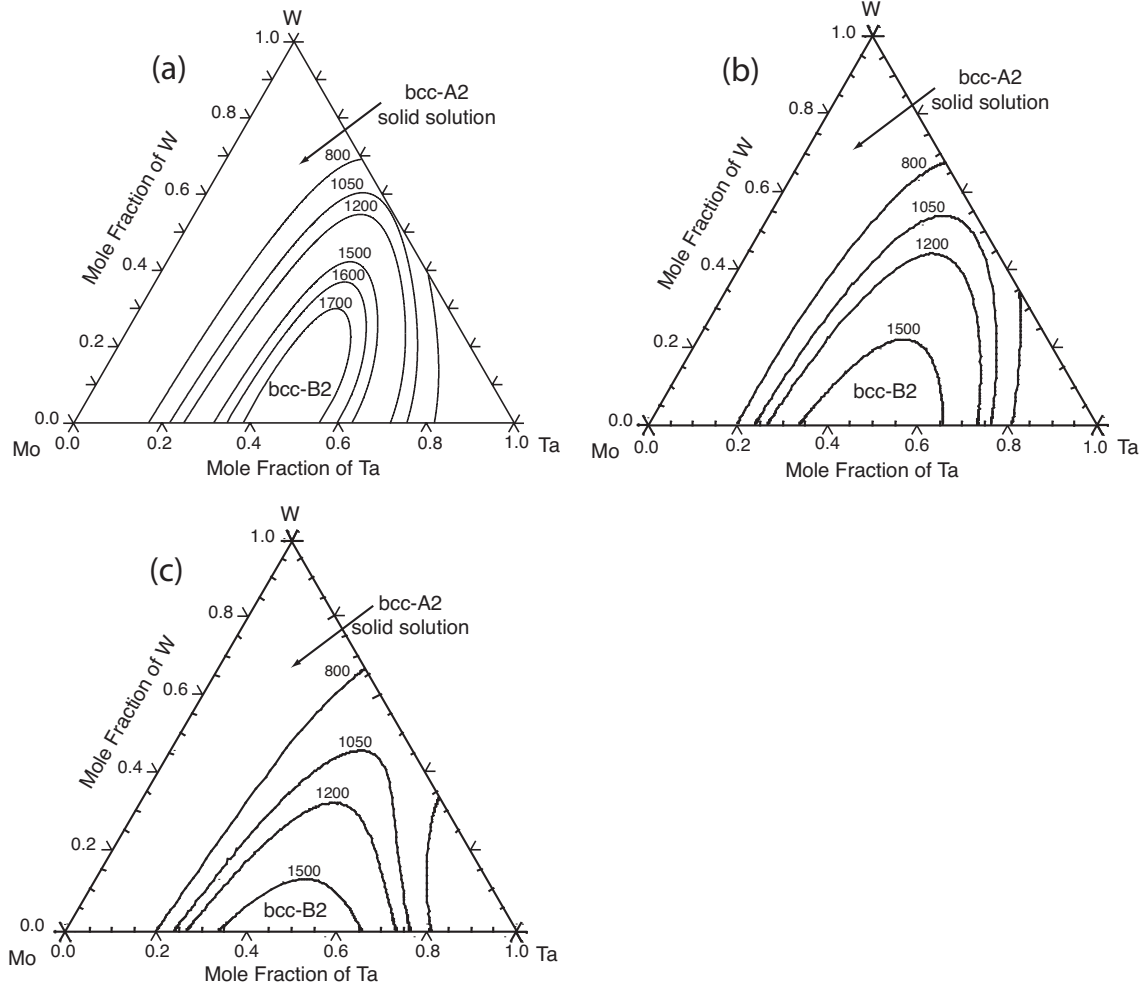


FIG. 10. Turchi et al.